BBA - Molecular Basis of Disease 1868 (2022) 166473

Contents lists available at ScienceDirect

BBA - Molecular Basis of Disease

journal homepage: www.elsevier.com/locate/bbadis

Rapid diagnosis of malignant pleural mesothelioma and its discrimination from lung cancer and benign exudative effusions using blood serum

Dilek Yonar [a,b], Mete Severcan [c], Rafig Gurbanov [d], Abdulsamet Sandal [e,f], Ulku Yilmaz [g], Salih Emri [e,h], Feride Severcan [a,i,*]

[a] Middle East Technical University, Department of Biological Sciences, Ankara, Turkey
[b] Yuksek Ihtisas University, Faculty of Medicine, Biophysics Department, Ankara, Turkey
[c] Middle East Technical University, Department of Electrical and Electronics Engineering, Ankara, Turkey
[d] Bilecik Seyh Edebali University, Department of Bioengineering, Bilecik, Turkey
[e] Hacettepe University, Faculty of Medicine, Department of Chest Diseases, Ankara, Turkey
[f] Ankara Occupational and Environmental Diseases Hospital, Ankara, Turkey
[g] Atatürk Chest Diseases and Chest Surgery Training and Research Hospital, Ankara, Turkey
[h] Medicana Hospital, Department of Chest Diseases, Kadikoy, Istanbul, Turkey
[i] Altinbas University, Faculty of Medicine, Biophysics Department, Istanbul, Turkey

ARTICLE INFO

Keywords:
Mesothelioma
Lung cancer
Blood serum
Spectral biomarkers
ATR-FTIR spectroscopy
Multivariate analysis

ABSTRACT

Malignant pleural mesothelioma (MPM), an aggressive cancer associated with exposure to fibrous minerals, can only be diagnosed in the advanced stage because its early symptoms are also connected with other respiratory diseases. Hence, understanding the molecular mechanism and the discrimination of MPM from other lung diseases at an early stage is important to apply effective treatment strategies and for the increase in survival rate. This study aims to develop a new approach for characterization and diagnosis of MPM among lung diseases from serum by Fourier transform infrared spectroscopy (FTIR) coupled with multivariate analysis. The detailed spectral characterization studies indicated the changes in lipid biosynthesis and nucleic acids levels in the malignant serum samples. Furthermore, the results showed that healthy, benign exudative effusion, lung cancer, and MPM groups were successfully separated from each other by applying principal component analysis (PCA), support vector machine (SVM), and especially linear discriminant analysis (LDA) to infrared spectra.

1. Introduction

Malignant mesothelioma is an aggressive form of cancer which arises from mesothelial cells lining pleural, pericardial, and peritoneal surfaces [1]. The well-known association between asbestos exposure and malignant mesothelioma was first defined in 1960 [2]. As the most common type of asbestos-related cancer, malignant pleural mesothelioma (MPM) accounts for approximately 80 % of all mesothelioma cases [3]. Usually, it is diagnosed later in life with a mean diagnostic age of 74 years and is four to eight times more common in males due to occupational asbestos exposure, but MPM prevalence is similar in both sexes due to environmental exposure to erionite, another naturally occurring fibrous minerals [4]. The prognosis for pleural mesothelioma depends on the factors such as tumor size and staging, histological type, gender, and age; when it is diagnosed, it has relatively poor median survival time of about 9–12 months [5]. The prevalence of MPM is reported to be 1.3/100,000 person-year for males, and 0.2/100,000 person-year for females all around the world. The statistics published in 2017 by the Republic of Turkey Ministry of Health revealed the age-standardized incidence rate of mesothelioma as 0.9/100,000 and 0.5/100,000 for males and females, respectively in Turkey [6].

The poor prognosis of MPM is related to the limited treatment options as well as poor diagnosis in the early stages and rapid progression of the disease with high invasiveness [7]. Signs and symptoms associated with MPM are nearly nonspecific and can be seen at almost any benign or malignant intrathoracic disease process. Therefore, the symptoms of this disease usually take decades to become noticeable. The latent period for the development of MPM after asbestos exposure might be up to 30–60 years [8]. So, the worst aspect of this disease is the timing. An early and accurate diagnosis of MPM is essential to decrease

* Corresponding author at: Altinbas University, Faculty of Medicine, Biophysics Department, 34147 Bakirkoy, Istanbul, Turkey.
E-mail addresses: feride.severcan@altinbas.edu.tr, feride@metu.edu.tr (F. Severcan).

https://doi.org/10.1016/j.bbadis.2022.166473
Received 19 December 2021; Received in revised form 6 June 2022; Accepted 19 June 2022
Available online 23 June 2022

the morbidity rate. The initial MPM diagnosis is usually based on imaging studies, including chest X-ray, computed tomography (CT), magnetic resonance imaging (MRI), and positron emission tomography (PET). Each imaging modality has its advantages and limitations, but their combined use is crucial in determining the individuals at high risk for MPM. However, the ultimate diagnosis of MPM depends on histological evidence including pleural fluid cytology obtained by thoracentesis and pleural tissue biopsy samples obtained during thoracoscopy or CT-guided fine-needle aspiration biopsy [9]. Pleural fluid may be analyzed by traditional biochemical methods. However, the most basic evaluation usually reveals a bloody effusion with increased lactate dehydrogenase (LDH) and protein levels according to Light's criteria, and even the cytology results are nonspecific and low in sensitivity, ranging from 0 % with a single sampling to 64 % with serial samplings [10]. Pleural tissue biopsy during thoracoscopy is an invasive process. CT-guided fine-needle aspiration is minimally invasive and limited by a small sample size, which reduces the sensitivity and increases the risk of pneumothorax (9.5 %) and needle tract seeding (21 %) [11]. Therefore, it would be critical to find new diagnostic approaches which are accurate, preferably non-invasive, rapid, low-cost, operator-independent and able to create reliable information.

Infrared (IR) spectroscopy (mid and near) is a highly suitable and preferred technique that can directly reflect the structural and functional changes induced by pathological or environmental conditions in biological systems ranging from cells to tissues and entire organisms [12–16]. It is a promising tool for the development of a clinically useful biomarker and ultimately enables early identification of diseases, because it allows monitoring disease-induced changes in vibrations of functional groups belonging to biomolecules. Attenuated total reflectance-Fourier transform infrared (ATR-FTIR) spectroscopy as a rapid, inexpensive, an easy-to-use, and operator-independent spectroscopic tool that can analyze even small amounts of samples, has had an important role in the field of disease diagnostics in recent years [17–19]. IR spectroscopy is a very suitable tool in the analysis of various biological materials, such as tissue sections, cytological and histological samples or biofluids [20]. In this context, biofluids like serum and plasma are ideal candidates for early detection of a wide range of diseases, since they are quite easily accessible and highly informative biofluids. Blood serum is a biological fluid that is commonly used in clinical practice and contains a lot of information about biomolecules such as protein, lipid, nucleic acid, etc. Besides, the low molecular weight fraction of the serum, peptidome, is thought to be a rich source of cancer-specific diagnostic information [21], making IR spectroscopic study of the serum ideal for detecting disease states as a triage tool. ATR-FTIR spectroscopy has been used in many studies as a promising analytical tool for cancer diagnosis from serum in a number of cancers [22–25]. Moreover, IR spectral measurements combined with multivariate analysis methods that provide significant information from complex and large spectral data are successfully employed in disease discrimination. Its combined use with multivariate analysis techniques has been widely applied in many cancer types involving lung [26], cervix [27], breast [28], ovarian [29], bladder [30,31], prostate [32], skin [33], and colon cancer [34]. Since novel robust algorithms for automated data analysis of large data sets have been developed to provide data interpretation easily by non-spectroscopists, FTIR spectroscopy can be progressed from “bench-to-bedside”. All these properties mentioned above make serum-infrared spectroscopy an excellent candidate for clinical translation.

While there is a great deal of literature on the applications of FTIR spectroscopy and microspectroscopy to lung cancer by using different types of biological samples [25,26,35–37], there are few articles on the applications of FTIR imaging and spectroscopy to mesothelioma in the literature. One of them is about the resolving of tumor subtypes in diffuse malignant mesothelioma by integrating FTIR imaging and laser capture microdissection. The authors proposed that FTIR imaging resolves not only morphological alteration within tissue but also it resolves even alterations at the level of single proteins in tumor subtypes [38]. Another study by our group is about the diagnosis of MPM from the pleural fluid using FTIR spectroscopy coupled with chemometrics [39]. In that study, it is proposed that FTIR spectroscopy coupled with multivariate analysis can improve and accelerate the discrimination of MPM from lung cancer and benign pleural effusion using pleural fluids. Since pleural fluids can be provided only from diseased individuals, in our previous study [39], we could not give any evidence or any information about the molecular mechanism of the diseases because there were no healthy control groups for comparison. In addition, the procedure of obtaining the pleural fluid has certain risks for major complications, including pneumothorax, chest wall hematoma, hemothorax, and tumor seeding to the chest wall in especially mesothelioma cases which do not occur during venous blood sampling to obtain serum [40]. Furthermore, only 15 % of cases with LC have pleural effusion in the beginning and 50 % develop pleural effusion during the entire course of the disease [41]. That is, pleural fluid occurs at the late stages of cancer. The advantage of using serum is that serum samples are readily available in each individual, regardless of pleural fluid status. Therefore, an early diagnosis from less invasive and easily collected blood serum is a very valuable approach. Adopting this method for serum samples avoids a dependency on having a pleural effusion and any risks of major complications associated with the thoracentesis procedure. Hence, serum studies are necessary to understand the molecular mechanism of the diseases.

In the present study, ATR-FTIR spectroscopy coupled with multivariate analysis methods was utilized to develop a new approach for the characterization and diagnosis of MPM and its differentiation from lung cancer (LC), benign exudative pleural effusions (BE), and healthy individuals via serum samples. Moreover, FTIR spectroscopy was employed to measure structural and contextual changes in the serum biomolecules of these different lung diseases in comparison to those of obtained from serum of healthy individuals, to understand their molecular mechanism. We also tested the hypothesis that IR spectroscopy could be used to identify biomarkers for MPM diagnosis and that it could provide new insights into the understanding of mechanisms underlying cancer and lung diseases.

2. Material and methods

2.1. Patients and sample collection

All methods, experimental protocols and experiments were approved following the requirements of research ethics boards (registration number HK 12/131-36, Hacettepe University Ethics Committee). Furthermore, informed consent of participants was obtained following the requirements of the research ethics boards, and all associated methods were conducted in accordance with approved guidelines and regulations for human biological specimens. The blood samples were transferred to the laboratory within 5 min of collection, and then centrifuged at 3000 rpm for 15 min to separate the serum from the cellular component. Serum samples were then transferred into cryogenic tubes and stored at −85 °C until the spectroscopy experiment [24].

The samples were collected from 25 malignant pleural mesothelioma (MPM) patients, 57 non-MPM individuals (26 individuals with non-malignant pleural effusions-benign exudative pleural effusion (BE)- and 31 individuals with lung cancer involving malignant pleural effusion), and from 30 healthy individuals (C). Healthy individuals were considered as control group. For the disease group, blood samples were collected prior to any invasive procedures. Demographic data of the studied groups and serum levels of LDH and Total Protein in patient groups are summarized in Table 1. The diagnosis of LC and MPM patients was made based on clinical, radiological, bronchoscopic findings and histopathological evaluation of biopsy specimens. The diagnosis of MPM was pathologically confirmed according to recommendations of Husain et al. [42] on both the appropriate morphology and

Table 1
Demographic data of healthy individuals and patients.

	Healthy individuals (C)	Benign exudative effusion (BE)	Lung cancer (LC)	Malignant pleural mesothelioma (MPM)
N	30	26	31*	25
Gender [n (%)]				
Male	19 (63.3)	15 (57.7)	20 (64.5)	15 (60.0)
Female	11 (36.7)	11 (42.3)	11 (35.5)	10 (40.0)
Age [median (range)]	37 (21–59)	54 (20–86)	62 (44–79)	60 (40–77)
Smoke status [n (%)]				
Current	4 (13.3)	13 (50.0)	12 (38.7)	5 (20.0)
Ex	5 (16.7)	0 (0.0)	0 (0.0)	0 (0.0)
Never	7 (23.3)	13 (50.0)	2 (6.4)	8 (32.0)
Not available	14 (46.7)	0 (0.0)	17 (54.8)	12 (48.0)
LDH (U/L)** [median (range)]	N/A	226.5 (138.0–439.0)	203.0 (125.0–756.0)	194.0 (2.0–431.0)
Total protein (g/dL)** [mean (SEM)]	N/A	7.2 (0.1)	6.9 (0.1)	7.1 (0.1)

* 25 Adenocarcinoma, 1 squamous cell ca, 3 non-small cell lung cancer of unspecified subtype, 1 adenosquamous carcinoma, 1 small cell ca.
The non-small cell lung cancer cases were in the metastatic stage.
The stage was extensive in the small cell lung cancer case.
** Serum LDH and total protein levels were retrospectively obtained from concomitant biochemical tests in 26 BE, 27 LC, and 21 MPM patients.

immunohistochemical findings obtained from adequate biopsy specimens. The diagnosis of BE was confirmed with the analysis of lactate dehydrogenase (LDH) and protein levels from pleural fluid and serum according to Light's criteria and with cytological tests [43,44]. There were not any significant differences in LDH levels and total protein levels among patient groups ($p > 0.05$).

2.2. Data collection and spectral analysis

Frozen serum samples were thawed and mixed at room temperature prior to spectroscopic analysis. Afterwards they were directly put on the ATR crystal and scanned. ATR-FTIR spectra of all samples was collected by one-bounce ATR mode of a Perkin Elmer Spectrum100 spectrometer (Perkin Elmer Inc., Norwalk, CT, USA) equipped with a Universal ATR accessory. 1 μL of serum samples were placed on a Diamond/ZnSe crystal plate and dried with a mild nitrogen gas flux for 2 min to remove excess unbound water. IR spectra of the samples were scanned in the 4000–650 cm^{-1} wavenumber region and 100 scans were taken for each interferogram with 4 cm^{-1} spectral resolution at room temperature. In order to eliminate the effects of water molecules in the air, the spectrum of air prior to sample spectra acquisition was recorded as a background under identical conditions as the samples and subtracted automatically from all the spectra. Perkin Elmer Spectrum software version 10.03.06 was utilized for recording the spectra and data manipulations. Three different randomly taken aliquots (1 μL each) from each serum sample were prepared and then scanned to check the reproducibility of identical spectra.

The average spectra of these replicates were used in further data analysis. These average spectra were baseline corrected and then normalized with respect to the amide I band for visual demonstration. The band positions were measured according to the center of mass [18]. For relative quantitative analysis, the integrated area ratios of some specific bands were evaluated in order to eliminate the artifacts that might arise from experimental conditions [45]. In order to calculate the integrated areas, first, interactive baseline correction of spectra was performed using the base points of the spectra. Then, the band area calculation relative to the obtained baseline was calculated for each group. The start and end abscissa values of the band and two base points were used to calculate the band areas.

2.3. Multivariate analysis methods

2.3.1. Unsupervised multivariate analysis methods

In order to discriminate the diseased groups from each other and the control group based on spectral differences, principal component analysis (PCA) was performed as an unsupervised multivariate analysis method. PCA is a data reduction technique that simplifies the evaluation of a large number of spectra. In practice, each spectrum consists of thousands of absorption values and can be considered as a point (or a vector) in a high dimensional space each coordinate of which corresponds to one of the variables (wavenumbers). PCA performs a linear transformation on this multidimensional space in such a way that most of the variations in the original space are preserved in the first few dimensions of the transformed space. This allows easier visualization or determination of spectra clusters representing different classes of samples. The coordinates of the transformed space are the principal components (PCs) and the plot obtained is called as scores plot [46]. PCs are ordered in such a way that the first PC, PC1, has the highest variation, the second PC, PC2, has the second highest variation, and so on. The transformation matrix consists of a set of orthogonal vectors called loadings. Loading scaled by the score value of the corresponding PC gives the contribution of that PC to the variation in the original spectrum.

In the current study, PCA was performed on the Unscrambler X, Version 10.3, (CAMO Software Inc., Oslo, Norway). Since one of the aims of this work was to identify MPM samples in different possible cases, different analyses were made over different intervals, such as 4000–650 cm^{-1}, 3050–2800 cm^{-1}, 1800–1500 cm^{-1}, 1800–900 cm^{-1}, 1480–900 cm^{-1}, 1200–1000 cm^{-1}. The input for Unscrambler X was, baseline corrected, normalized spectra over these intervals or their first derivatives or second derivatives [47].

2.3.2. Supervised multivariate analysis methods

The supervised methods require a number of well-characterized training and test samples to obtain class models. They comprise a two-step process as calibration and validation. In the calibration stage, each sample is identified as a member or not of a determined class, in accordance with the previous characterization of the samples. The aim is to calibrate a prediction/classification model which will be used to classify or predict new and non-characterized samples. In the validation stage, the calibrated model is tested and validated [48].

SVM is a supervised classification method. In principle, SVM determines the optimum hyperplane that separates two groups of points (vectors) which are separable in a multidimensional space. The sample points closest to this hyperplane are called support vectors. The support vectors have the property that they have the same distance to this plane. If the sample points cannot be separated by a hyperplane into two groups, the SVM algorithm determines the best possible hyperplane. If the groups are not separable by a hyperplane but by some other hypersurface, a transformation can be used to obtain, effectively, a hyperplane that separates the two groups. To classify more than two groups, the SVM algorithm can still be used by applying it to pairs of groups [49–51].

In this work the "Classification Learner App" of MATLAB, R2019a,

was used to implement SVM. The input to SVM was the 10-dimensional scores vectors obtained from the PC analysis of serum sample spectrograms using Unscrambler X. The app allows up to 50 folds of cross validation. Therefore, for sample sizes <50, full cross-validation was possible. For a higher number of sample sizes, the SVM algorithm was repeated several times to obtain the best possible classification. MATLAB classification app outputs a model which can be used to classify any new serum sample spectrogram. The required scores vector of the new sample can be calculated using the same transformations obtained during the PC analysis. To evaluate the performance of the SVM classification and confusion tables of the true positive and false negative rates were used.

LDA is another supervised method. The PCA data, offset baseline corrected and unit vector normalized over all column range (1–3351) were used as LDA model inputs over 1300–800 cm^{-1} spectral range using The Unscrambler X 10.3 (CAMO Software AS, Norway) multivariate analysis software. The category variable column was included in a data matrix, and, subsequently, all spectra of different sample categories were used to build a training set. Quadratic classifiers method using projections of 14 PCA components were applied for prediction. Prior probabilities were calculated from the training set [52,53]. The results are presented as a discrimination plot as well as prediction and confusion matrices.

2.4. Statistics

Spectral results for all groups were expressed as mean ± standard error of the mean (SEM). The data were evaluated using a normality test to decide whether the parametric or nonparametric statistical test should be used. Serum LDH and Total Protein levels were compared among patient groups using the Kruskal-Wallis test and one-way ANOVA tests, accordingly. Since other data showed normal distribution, the patient groups versus the control group were analyzed using the one-way ANOVA and Dunnett's multiple comparison tests in GraphPad Prism 6 (GraphPad Software, Inc.). $p < 0.05$ was considered as statistically significant. The degree of significance for the comparison of the diseased groups with respect to the control group was denoted as $*p < 0.05$, $**p < 0.01$, $***p < 0.001$, and $****p < 0.0001$.

3. Results

The aim of the current study is to develop a new approach for the characterization and diagnosis of MPM and its differentiation from LC, BE patients and healthy individuals via serum samples. We performed ATR-FTIR spectroscopy to characterize and differentiate healthy individuals, benign and malign exudative effusions by serum analysis. Fig. 1A–B displays the averaged FTIR spectra of the serum samples of controls and patients (BE, LC and MPM) in the 3000–2800 and 1800–650 cm^{-1} regions where the characteristic absorption bands arising from the functional groups of various biomolecules such as lipids, proteins, carbohydrates and nucleic acids (RNA/DNA) are assembled. The absorption bands, the contributions from the functional groups of biomolecules labeled in Fig. 1A–B and their assignments according to the related literature [20,54–56] are summarized in Table 2. In order to see the differences more clearly between the samples, difference spectra were obtained, where the average spectrum of each disease group namely BE, LC and MPM was subtracted from the average spectrum of the control in the 3000–2800 and 1800–650 cm^{-1} regions (subpanels in Fig. 1A–B). There are obvious spectral differences in the functional groups of the biomolecules of the serum samples obtained from LC and MPM patients compared to the controls and BE patients (Fig. 1). The amide modes of proteins located at 1635 cm^{-1} and 1538 cm^{-1} indicate a slight difference in the proteins of the diseased groups' samples. The most prominent differences are observed in the 1300–800 cm^{-1} spectral range which is dominated by absorptions from amino acids of proteins, carbohydrates, DNA and RNA (Fig. 1). Hence, it is

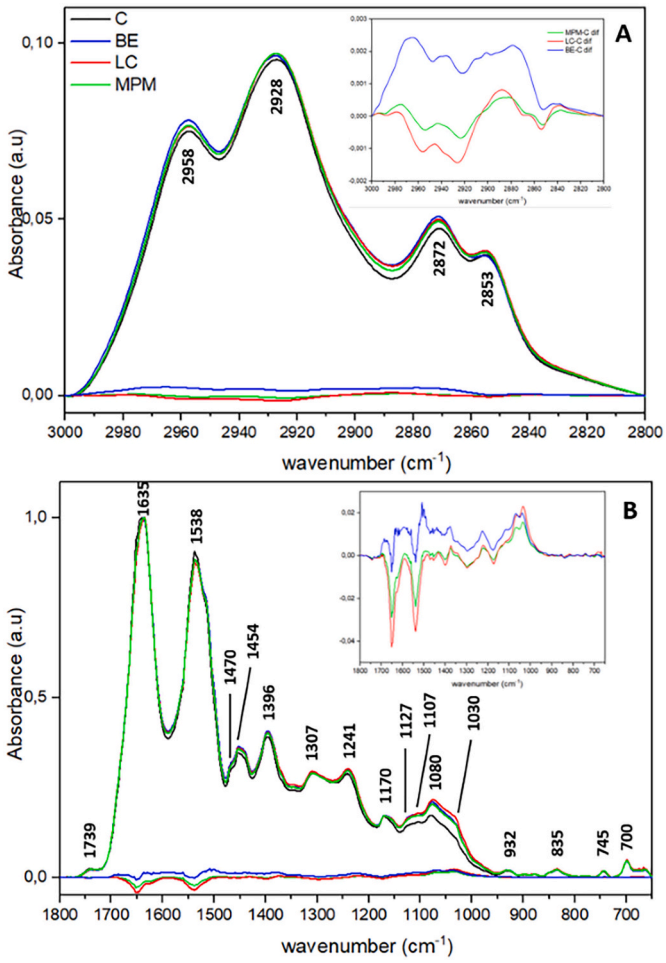

Fig. 1. The average serum spectra of the studied groups in the A) 3000–2800 and B) 1800–650 cm^{-1} regions. The spectra were normalized with respect to the amide I band located at 1635 cm^{-1}. Difference IR spectra were obtained by the subtraction of the control spectrum from the disease groups' spectra in the subpanels for both regions. Healthy control (black), benign exudative effusion (blue), lung cancer (red) and malign pleural mesothelioma (green).

important to perform a detailed spectral analysis to determine specific disease-induced changes and to find out disease biomarkers. To get the quantitative differences in the spectral bands of the studied groups, spectral band areas and area ratios for specific bands were calculated from their absorbance spectra considering the literature [18,25,39,57,58] and are presented in Table 3. In accordance with Beer-Lambert law, signal intensity/area under the spectral bands is directly proportional to the concentration of the functional groups belonging to the relevant molecule. Moreover, the structural information about the relevant molecule can be obtained by the variations in their band positions [14,18].

An IR spectrum of a biological sample mainly covers C—H stretching (3000–2800 cm^{-1}) and molecular fingerprint (1800–650 cm^{-1}) regions. The antisymmetric and symmetric stretching of methylene ($–CH_2$) and methyl ($–CH_3$) group vibrations in the C—H region are mainly lipid-associated spectral bands as given in Fig. 1. The bands at nearly 2928 (CH_2 antisymmetric stretching) and 2852 cm^{-1} (CH_2 symmetric stretching) belonging to aliphatic $–CH_2$ functional groups stem from long hydrocarbon chains in lipids. The area ratio of CH_2 sym to CH_2 antisym + CH_2 sym corresponds to saturated lipid content and its increase indicates the higher lipid content [45]. In addition, the molecular fingerprint region also contains some considerable lipid-associated spectral bands such as CH_2 bending mode and the C═O stretching mode of the acyl chains of lipids located at 1470 and 1739 cm^{-1},

Table 2
The band assignment of an IR spectrum for serum sample.

Wavenumber (cm^{-1})	Band Assignment
3284	Amide A band due to N—H stretching: protein
3062	Amide B band due to overtone of Amide I: protein
2958	CH_3 antisymmetric stretching: protein, lipid
2928	CH_2 antisymmetric stretching: mainly lipid
2872	CH_3 symmetric stretching: mainly protein
2853	CH_2 symmetric stretching: mainly lipid
1739	Ester C═O stretching: triglyceride, cholesterol esters
1635	Amide I band mainly due to C═O stretching vibration of amide groups: protein
1538	Amide II band due to N—H bending strongly coupled to C—N stretching vibration of amide groups: protein
1470	CH_2 bending: lipid
1454	CH_3 antisymmetric bending: protein
1396	COO^- symmetric stretching: fatty acids and aminoacids
1307	Amide III: C—N stretching and N—H bending
1241	PO_2^- antisymmetric stretching: mainly nucleic acid with a little contribution of phospholipids
1170	C-OH antisymmetric stretching: serine, threonine and tyrosine aminoacids of proteins
1127	C—O stretching: ribose
1107	P—O—C symmetric stretching: DNA
1080	PO_2^- symmetric stretching: nucleic acids and phospholipids
1030	C—O stretching: carbohydrates (glycogen, glucose)
932	Z-form DNA
835	A-form and B-form helix conformation of DNA

Table 3
The area ratio between the areas of the selected band and their indications.

Area ratio	Biomolecular origin*	Indication
A_{2928}/A_{2958}	CH_2 as υ/CH_3 as υ	Aliphatic chain length
$A_{2853}/A_{2928+2853}$	CH_2 s υ/(CH_2 as υ + CH_2 s υ)	Saturated lipids content
$A_{1739}/A_{2928+2853}$	Ester C═O υ/(CH_2 as υ + CH_2 s υ)	Triglyceride-cholesterol ester amount
A_{1635}/A_{1538}	Amide I/amide II	Protein structural and conformational changes
$A_{1635}/A_{1635+1538}$	Amide I/(amide I + amide II)	Protein concentration
$A_{2928+2853}/A_{1635+1538}$	(CH_2 as υ + CH_2 s υ)/(amide I + amide II)	Lipid/protein content
$A_{1240+1080}/A_{1635+1538}$	(PO_2^- s υ + PO_2^- as υ)/(amide I + amide II)	Nucleic acid/protein content
A_{1127}/A_{835}	C—O υ/C2′ endo/anti-conformation	RNA/DNA content
$A_{835}/A_{1240+1080}$	C2′ endo/anti conformation/(PO_2^- s υ + PO_2^- as υ)	DNA concentration
$A_{1030}/A_{1635+1538}$	C—O υ/(amide I + amide II)	Glucose/protein content

* Abbreviation: as = antisymmetric, s = symmetric, υ = stretching.

respectively. The area ratios of specific lipid functional groups to the total lipid content were calculated to analyze the disease-induced changes in the molecular composition and structure of lipids (Table 3). The methylene/methyl (CH_2/CH_3 antisym. stretch.) area ratio gives information about acyl chain length. Its higher value implies the presence of comparatively longer chained lipids, whereas its lower value means the presence of shorter chained and/or more branched ones [39,57,58]. The carbonyl/lipid ratio indicates the triglycerides and cholesterol ester content in the sample. The band area ratio values of the lipid related peaks are shown in Fig. 2A–C. The band area ratio of the CH_2 sym. stretch. to total saturated lipids, the carbonyl/lipid ratio and methylene/methyl ratio were found to be significantly higher in the serum of LC and MPM groups compared to the BE and control groups. The changes in these lipid functional groups demonstrated the higher lipid content, the presence of qualitatively longer hydrocarbon acyl chained lipids, and the higher triglyceride and cholesterol ester amount in the serum of both LC and MPM groups relative to the control and BE groups, respectively (Fig. 2A–C). Furthermore, the wavenumber of the CH_2 antisymmetric bands shifted significantly towards lower values in the malignant serum samples in comparison to the serum samples of control and BE (Table 4). This shift towards lower values implies an increase in lipid order e.g. the less flexible lipid acyl chains for LC and MPM patients [45].

The band located around 1635 cm^{-1} (amide I) is a well-known protein band [59]. The location of amide I band (1635 cm^{-1}) indicates that serum proteins are mainly in beta sheet structure as also reported in other serum studies [53]. The band located around 1540 cm^{-1} (amide II) is also well-known protein band [53]. The disease-induced changes in the protein amount are calculated from the area ratios of amide I to amide I + amide II bands (Table 3). No significant changes were observed in this ratio. However, a decrease in the area of all amide modes, the functional groups of the proteins, were observed. Furthermore, as seen in Fig. 2D, the lipid/protein ratio increased significantly in the serum samples of the malignant groups (LC and MPM) ($p < 0.001$) compared to the control group. The amide I/amide II area ratio and the position of these absorption peaks are sensitive to protein structural and conformational changes. This is because, amide I and amide II bands originate from different functional groups of proteins (Fig. 1). A highly significant decrease in the wavenumber of the amide I band, indicating alterations mainly in C═O stretching vibration of amide groups in proteins (Table 4). Furthermore, the amide I/amide II area ratio was evaluated and no remarkable structural changes were observed between the groups.

The vibrations from PO_2^- functional groups originate mainly in the phosphodiester groups of nucleic acids (Fig. 1) and the increased absorption in these bands suggests an increase in nucleic acids in malignant tissues [60]. PO_2^- groups of phospholipids have little contribution to these bands. Integrated area in the phosphates of nucleic acids measured by integrating the symmetric and antisymmetric vibrations of PO_2^- functional groups at around 1080 and 1240 cm^{-1} and their band positions were evaluated. Significant shifts to lower values of the PO_2^- antisymmetric stretching band position were found for BE, LC and MPM groups with respect to the control group, indicating the conformational changes in the nucleic acids (Table 4). An increase in the phosphate level of nucleic acids for malignant serum samples (LC, MPM) was obtained. Moreover, nucleic acid/protein ratios in the serum of control, BE, LC and MPM groups are shown in Fig. 2E and the observed increase ($p < 0.0001$) in this ratio of the diseased groups suggests an increased nucleic acid content in comparison to proteins of the patients. RNA/DNA area ratio was calculated as given in Table 3 and shown in Fig. 2F. This ratio for BE group remained almost the same as in control serum samples, while it tended to increase in malignant serum samples and it was found significantly higher in the serum samples of MPM patients. As seen in Fig. 2G, DNA concentration was calculated as explained in Table 3 and this ratio was found significantly low in the malignant groups. Since the band area ratio related to DNA concentration decreased in the malignant groups, the increase in the band area ratio values of RNA to DNA may be due to this decrease in DNA content (Fig. 2F,G). Although there was an almost similar decrease in DNA concentration in malignant groups, the RNA/DNA ratio increased more in MPM indicating an increased amount of RNA in MPM.

Quantitative analysis of glucose has frequently been achieved using the spectral band at 1030 cm^{-1} which is related to C—O stretching of carbohydrates especially for glucose [39,61–63]. Fig. 2H demonstrates the carbohydrate level with respect to the protein amount. This area ratio increased for all groups as compared to the control (Fig. 2H).

The results of Fig. 2 indicate that spectral parameters such as the higher saturated lipid content, the presence of qualitatively longer hydrocarbon acyl chained lipids, the higher triglyceride-cholesterol ester amount and increased lipid/protein ratio in the serum of both LC and MPM groups relative to the control and BE groups can be used as biomarkers in cancer diagnosis. Despite this, RNA/DNA ratio was significantly higher only for MPM group, therefore, this ratio can be used as a

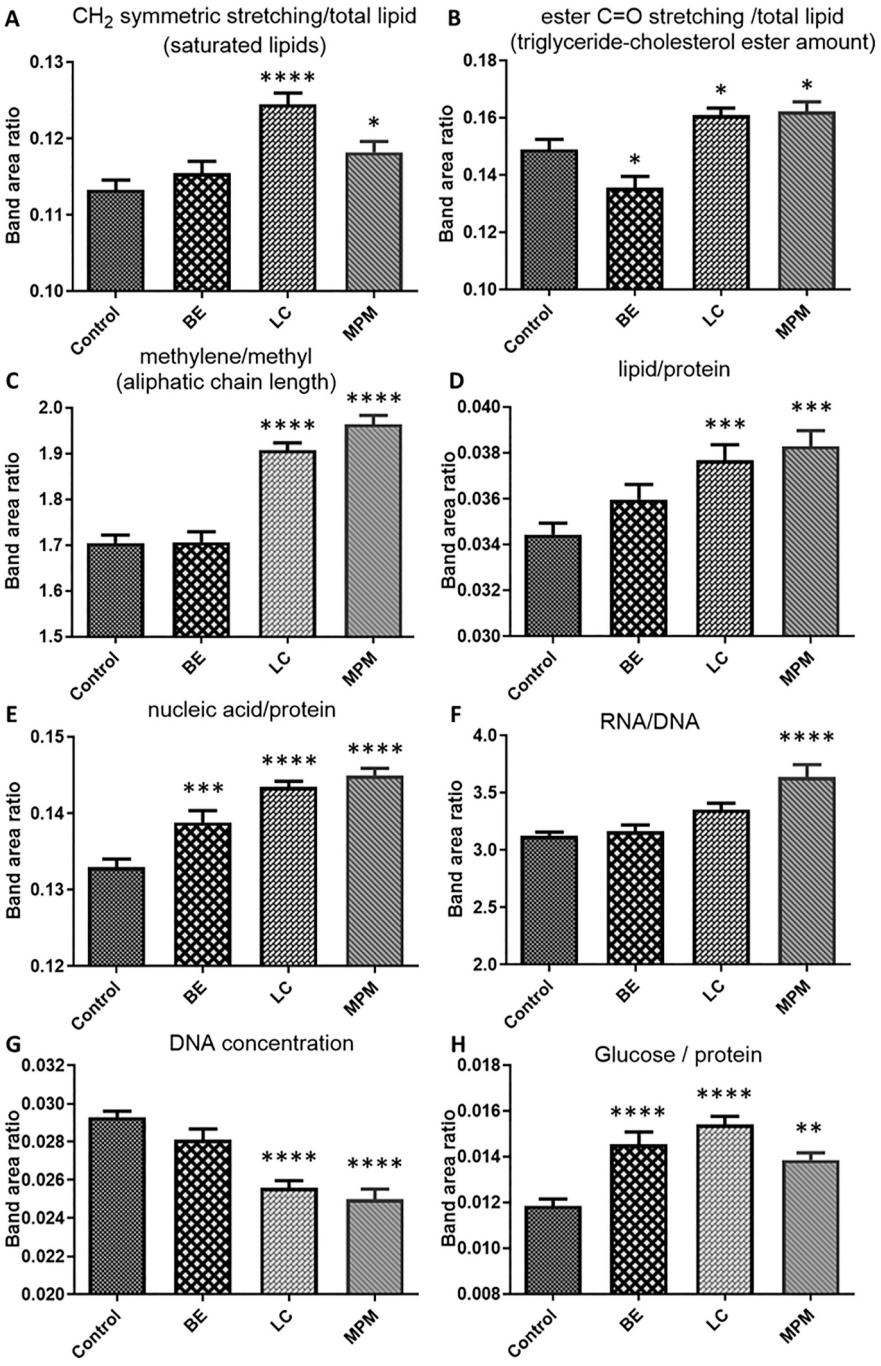

Fig. 2. Bar graphs of A) saturated lipid amount, B) ester carbonyl/total lipid, C) methylene/methyl, D) lipid/protein, E) nucleic acid/protein, F) RNA/DNA, G) DNA concentration and H) glucose/protein area ratios of control, BE, LC and MPM groups (The degree of significance for the comparison of the diseased groups with respect to the control group was denoted as $*p < 0.05$, $**p < 0.01$, $***p < 0.001$, $****p < 0.0001$).

specific biomarker in the MPM diagnosis.

In addition to the spectral characterization studies, meaningful diagnostic information can be obtained by the multivariate analysis methods applied to IR spectra. First, principal component analysis (PCA) as an unsupervised method was applied. The mean-centered PCA was conducted over the whole region, 3100–2800, 1800–650, 1200–800, 1100–900 and 1350–1100 cm^{-1}spectral regions. When the PCA is performed on all of the samples of four groups it was not possible to observe discrimination of different groups by considering only 2 or 3 dimensional scores plots due to a great deal of overlap of different groups. Therefore, we adapted a multistage classification strategy by eliminating possible classes step by step considering PCA of 4-group, 3-group and 2-group combinations. For example, as seen from the scores plot of the PCA of all 4 groups shown in Fig. 3A, control samples are easily discriminated from the other 3 disease groups, BE, LC and MPM. Therefore, the next step will be a search in 3-group combination for a malign sample. Some examples for the discrimination of different group combinations are presented in Figs. S1 and S2 of the Supplementary Material. Fig. S1 shows the scores plots for the group combinations C-LC-MPM and LC-MPM. PCA scores plots for BE-LC-MPM, BE-MPM and BE-LC group combinations are given in Fig. S2. The PCA scores plots shown in Fig. S1A demonstrated that the clusters of LC and MPM serum samples were clearly separated from the control samples. From Fig. S1B, it is observed that malign groups, LC and MPM, can be differentiated from

Table 4
Changes in the wavenumbers of lipid, protein, carbohydrate and nucleic acids related functional groups.

Band assignment	Wavenumber (cm^{-1})									
	Control		BE			LC			MPM		
	Mean	SEM	Mean	SEM		Mean	SEM		Mean	SEM	
CH_2 antisym. stretch.	2929.19	0.22	2929.04	0.23		2928.44	0.16	↓*	2928.48	0.17	↓*
Ester C═O stretch.	1740.01	0.23	1739.64	0.33		1739.49	0.34		1739.60	0.32	
Amide I	1638.92	0.33	1637.43	0.43	↓*	1636.84	0.29	↓***	1637.71	0.35	↓*
Amide II	1536.81	0.28	1535.95	0.30		1536.81	0.19		1536.95	0.33	
PO_2^- antisym. stretch.	1240.64	0.28	1236.05	0.75	↓****	1236.94	0.60	↓****	1237.87	0.56	↓**
C-OH antisym. stretch.	1171.72	0.02	1171.65	0.03		1171.66	0.02		1171.67	0.02	
C—O stretch. (RNA)	1127.83	0.03	1127.35	0.07	↓****	1127.66	0.06	↓*	1127.70	0.06	↓*
C—O stretch. (glucose)	1029.94	0.06	1029.77	0.09		1030.04	0.05		1030.15	0.10	

The degree of significance for the comparison of the diseased groups with respect to the control group was denoted as * $p < 0.05$, ** $p < 0.01$, *** $p < 0.001$, **** $p < 0.0001$.

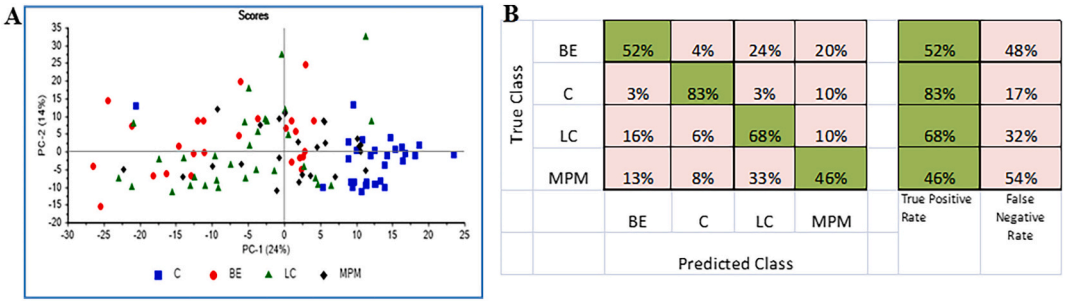

Fig. 3. A) Scores plot in PC1–PC2 plane for the spectral region 1480–900 cm^{-1}, for all samples, C, BE, LC and MPM. B) Confusion table for the classification model obtained from SVM.

each other. Moreover, the discrimination of LC and MPM groups from benign exudative effusions (BE) was analyzed and a clear separation between BE and malign groups as two clusters was obtained in the 3050–2800 cm^{-1} spectral region (Fig. S2A). The differentiation of MPM and LC groups from BE group was also examined separately (Fig. S2B, C).

Furthermore, in order to investigate the diagnostic significance of classification of MPM from the IR spectrums of serum samples, two supervised multivariate analysis methods, support vector machine (SVM) and linear discriminant analysis (LDA), were performed. SVM was applied to the 10-dimensional scores vectors obtained from the PCA of samples as described in the method section above. Classification was done for the following possible cases: 1. {C, BE, LC, MPM}, 2. {BE, LC, MPM}, 3. {BE, MPM}, 4. {LC, MPM}. The first case assumes no prior knowledge of the presence of any of the 4 possible groups. The second case assumes that one of the 3 diseases is possible. In the third and fourth cases it is assumed that one of the two diseases is possible. For each case, for different regions of the spectrum, classification performance was obtained for normalized spectra, first and second derivative spectra. Best results were obtained for the 1480–900 cm^{-1} region of the spectrum which includes RNA-DNA bands. For PCA, this region of the spectrum was first baseline offset corrected, then peak normalized with respect to the peak at 1240 cm^{-1}. In addition to the normalized spectrum, 1st and 2nd derivatives of the normalized spectra were obtained using Savitzky-Golay method with 9-point smoothing. In the following, PCAs were performed with full cross-validation.

For the first case of 4 different groups, Fig. 3A shows the scores plot for the first 2 PCs of the 2nd derivative spectrum. As seen from the scores plot most of the Control samples are clustered together while MPM samples are highly scattered among other groups. The confusion table of the classifier model obtained from a linear SVM classifier is shown in Fig. 3B. Only 46 % of the MPM samples were correctly classified. It should be mentioned here that if the BE, LC, and MPM samples were combined into a single disease class D, a two class SVM classifier, to discriminate D from C, yields a classification model which has a 99 % true positive rate for class D. In other words, SVM separates the disease samples from control samples almost perfectly.

In LDA classification, the best performance was obtained for 1300–800 cm^{-1} spectral region. However, comparable predictions were also obtained for 1480–900 cm^{-1} as well as 4000–650 cm^{-1} regions.

For the first case of 4 different groups, LDA prediction was obtained with 87.5 % accuracy as shown in the discrimination plot (Fig. 4A). As can be seen from the prediction (Table S1) and confusion (Fig. 4B) matrices, the great majority of actual individuals were correctly predicted/classified in their corresponding classes: 30 out of 30 for C, 18 out of 26 for BE, 31 out of 31 for LC and 19 out of 25 for MPM.

For the 2nd case of 3 disease groups, {BE, LC, MPM}, the best classification was obtained from a PCA over the interval 1480–900 cm^{-1} using the 2nd derivative of peak normalized spectra described above. Scores plot, in PC1–PC2 plane, obtained from PCA is given in Fig. S3. The classifier model obtained by using a linear SVM classifier has the true positive rates of 44 %, 68 % and 50 % for BE, LC, and MPM groups respectively.

LDA results for the 2nd case of 3 disease groups (BE, LC and MPM) are shown in Fig. 5. The accuracy of the discrimination in the developed model was 82.93 % (Fig. 5A). The 18 actual BE patients out of 26, 31 LC patients out of 31, and 19 MPM patients out of 25 were correctly predicted in their corresponding classes (Table S2). As it is seen from Fig. 5B, 8 samples out of 26 of BE group were false positively diagnosed. These false positives in the benign group were patients with more pronounced inflammatory conditions including systemic lupus erythematosus, ankylosing spondylitis, tuberculous pleurisy, and parapneumonic infection.

For the 3rd case of BE and MPM groups only, i.e. assuming that LC is known to be not existing, the best SVM classifier is obtained by using a linear SVM on the scores vectors obtained from a PCA using 2nd derivative spectra over the spectral range 1480–900 cm^{-1}. Fig. 6A, B (left panel) shows the PCA scores plot and the confusion table for the

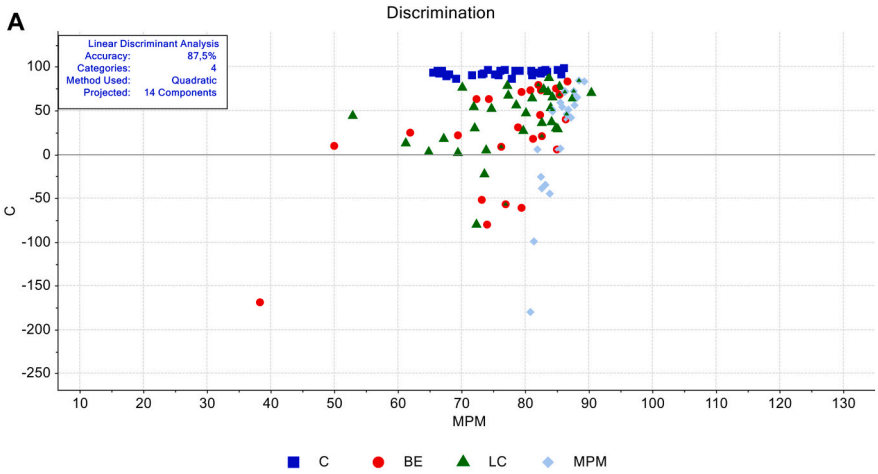

B

Confusion m	Actual	C	BE	LC	MPM
Predicted		1	2	3	4
C	1	30	0	0	0
BE	2	0	18	0	0
LC	3	0	6	31	6
MPM	4	0	2	0	19

Fig. 4. The discrimination of the serums obtained from healthy control (C), benign exudative effusion (BE), lung cancer (LC), and malign pleural mesothelioma (MPM) individuals by supervised LDA. (A) The discrimination plot obtained in 1300–800 cm^{-1} spectral region for the aforenamed groups. (B) Confusion matrix of the model classes.

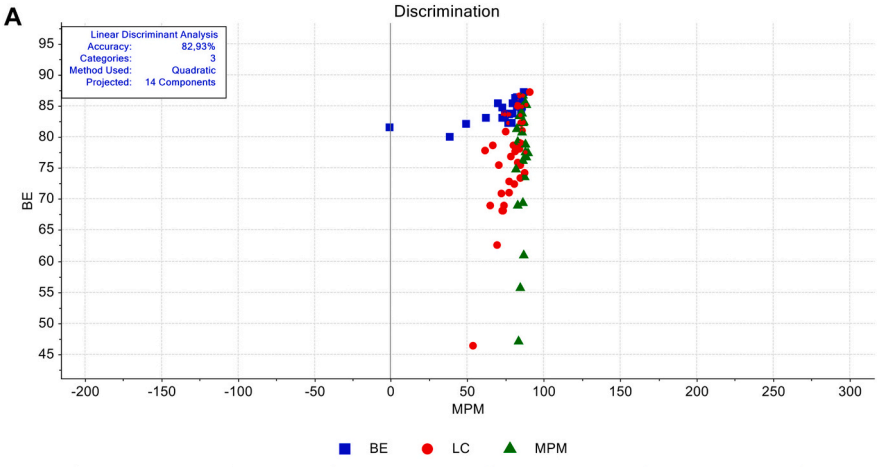

B

Confusion m	Actual	BE	LC	MPM
Predicted		1	2	3
BE	1	18	0	0
LC	2	6	31	6
MPM	3	2	0	19

Fig. 5. The discrimination of the serums obtained from benign exudative effusion (BE), lung cancer (LC), and malign pleural mesothelioma (MPM) individuals by supervised LDA. (A) The discrimination plot obtained in 1300–800 cm^{-1} spectral region for the aforenamed groups. (B) Confusion matrix of the model classes.

classifier model obtained.

For the last case of LC and MPM groups only, i.e. assuming that BE is known to be not existing, the best SVM classifier is obtained by using an SVM classifier having a cubic kernel on the scores vectors obtained from a PCA using 1st derivative spectra over the spectral range 1480–900 cm^{-1}. Fig. 6C, D (right panel) shows the PCA scores plot and the confusion table for the classifier model obtained.

In the 3rd case of BE and MPM groups, the discrimination accuracy of the LDA model was 94.12 % (Fig. 7A). As shown in prediction and confusion matrices, 24 out of 26 and 24 out of 25 actual patients were correctly predicted as BE and MPM class members, respectively. However, 2 BE patients were predicted as MPM patients and 1 MPM patient was classified as BE patient (Table S3, Fig. 7B). The LDA model was developed with 91.07 % accuracy for the last case of LC and MPM groups (Fig. 8A). All 31 actual LC patients were correctly predicted as LC patients, however, the number of correctly predicted MPM patients were

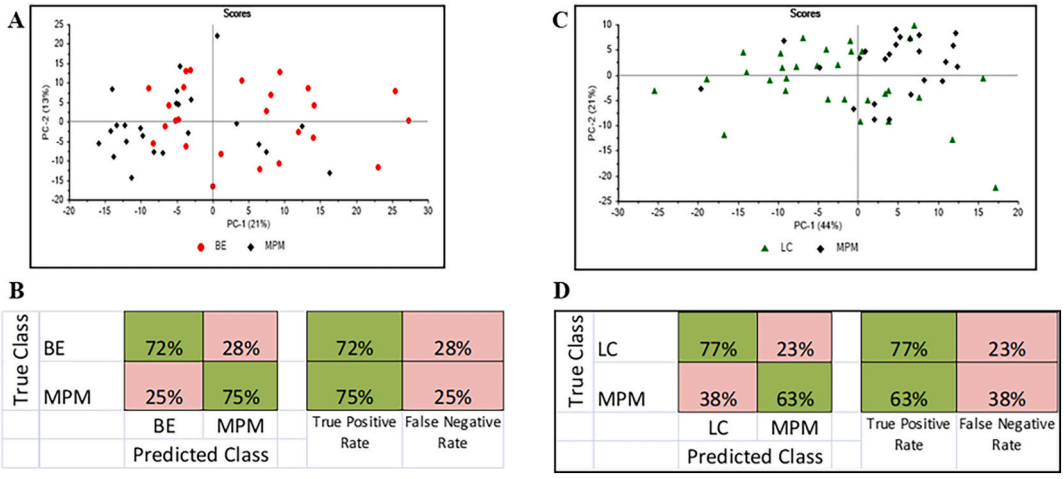

Fig. 6. A) PCA scores plot for {BE, MPM} samples using 2nd derivative spectra over the spectral range 1480–900 cm^{-1}. B) Confusion table and C) PCA scores plot for {LC, MPM} samples using 1st derivative spectra over the spectral range 1480–900 cm^{-1}. D) Confusion table.

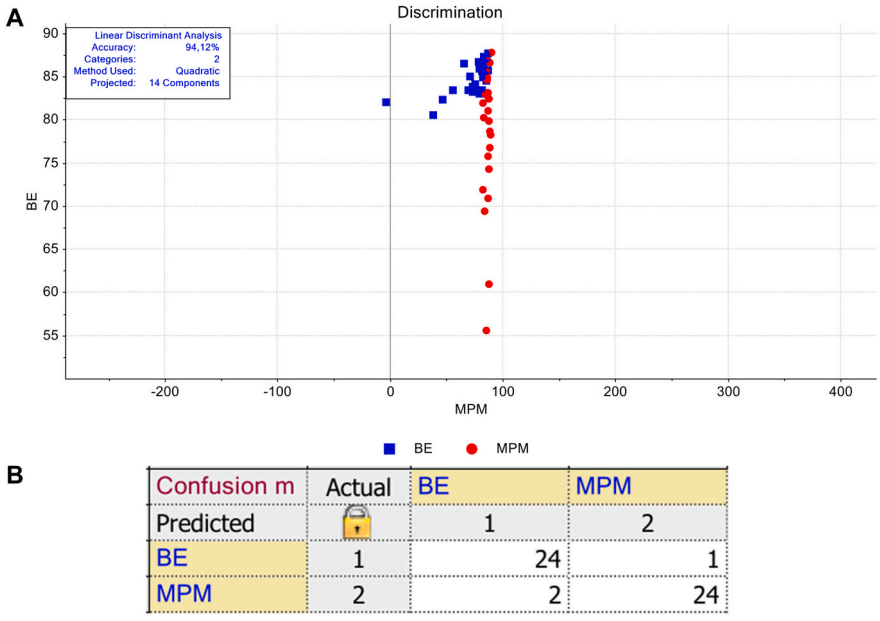

Fig. 7. The discrimination of the serums obtained from benign exudative effusion (BE) and malign pleural mesothelioma (MPM) individuals by supervised LDA. (A) The discrimination plot obtained in 1300–800 cm^{-1} spectral region for the aforenamed groups. (B) Confusion matrix of the model classes.

20 out of 25 (5 actual MPM patients were predicted as LC) (Table S4, Fig. 8B).

4. Discussion

In the present study, we used human blood-serum to perform characterization and discrimination analysis of benign and malign exudative pleural effusions and healthy controls by using ATR-FTIR spectroscopy coupled with chemometrics. The importance of serum studies in MPM was reported in a recent article [64]. In this review article, it was reported that most frequently (65 %) assessed matrix is serum due to its certain advantages [64]. First, these studies can include healthy controls together with patients groups. Second, venous blood sampling is devoid of major complications which can occur during or after thoracentesis [65]. Third, repetitive testing with blood samples for confirmation or during the patient follow-up is easier, moreover it does not contain a risk for procedure tract metastasis, which may occur due to seeding of tumor cells during the sample obtaining [66]. It is not clinically recommended when the potential complication of the procedure outweigh the benefits, therefore, effective blood tests can be preferable in the differential diagnosis of pleural effusions. Thus, routine, inexpensive, less invasive, and safer acquisition of biological materials like blood/serum with reliable results can be advantageous for diagnostic and management purposes.

FTIR spectroscopy can directly reflect the structural and functional changes induced by pathological or environmental conditions in biological systems. There are spectral differences in the serum samples obtained from LC and MPM patients compared to the controls and BE patients. The observed results such as the higher lipid content, the presence of qualitatively longer hydrocarbon acyl chained lipids and the higher triglyceride and cholesterol ester amount in the serum of both LC and MPM groups relative to the control and BE groups might be due to the higher lipid biosynthesis. It has been accepted that lipid metabolism is involved in many aspects of cancer cell biology as a major metabolic pathway. The principles underlying the production of lipids, as well as nucleic acids and protein biosynthesis can provide important insights

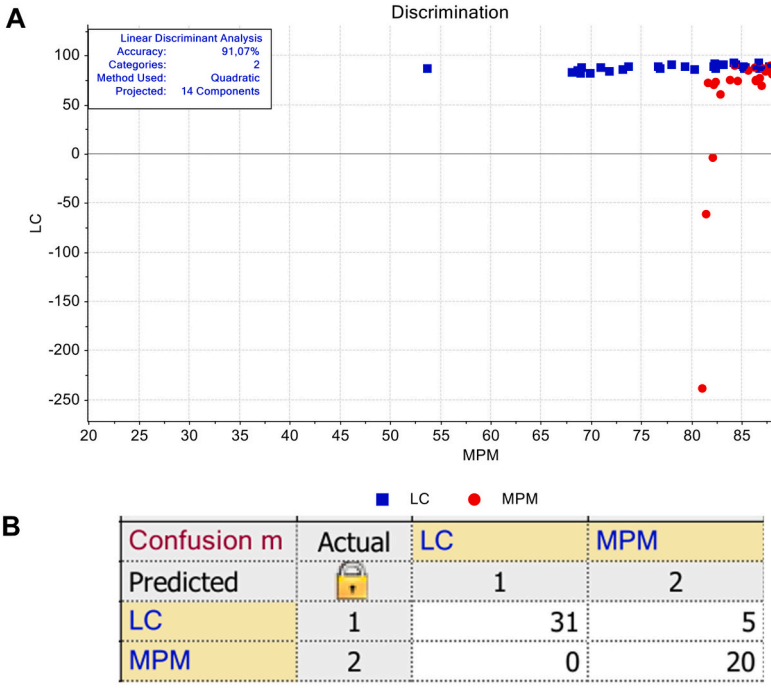

Confusion m	Actual	LC	MPM
Predicted		1	2
LC	1	31	5
MPM	2	0	20

Fig. 8. The discrimination of the serums obtained from lung cancer (LC) and malign pleural mesothelioma (MPM) individuals by supervised LDA. (A) The discrimination plot obtained in 1300–800 cm^{-1} spectral region for the aforenamed groups. (B) Confusion matrix of the model classes.

into the understanding of cell growth and proliferation. Lipids also play an active role in the signaling processes which is involved in cell transformation and tumor development [67]. Abnormal levels of lipids are closely linked to carcinogenesis and metastasis of many cancer types. High expression of fatty acid synthase, an important enzyme that catalyzes the synthesis of endogenous long chain fatty acid has been observed in cancer cells [68]. Fatty acid synthase overexpression in mesothelioma tissues was reported by Gabrielson et al. [69], confirming the higher lipid synthesis and thus our results. Increased triglyceride amount in serum of LC and MPM patients that we have found was also consistent with those demonstrated in recent studies as elevated plasma, serum and pleural fluid triglyceride levels in lung, breast cancer and mesothelioma patients [39,70–72]. The lipids in the body fluids of mesothelioma and gastric cancer patients were also reported as relatively longer acyl chained than the lipids in healthy individuals, verifying our result indicating the presence of qualitatively longer hydrocarbon acyl chained lipids in the serum of both LC and MPM groups (Fig. 2A–C) [39,58].

The slight decrease observed in all the amide modes indicates a decrease in protein content. The increase in the lipid/protein ratio is mostly attributed to a higher lipid content, indicating an alteration in the lipid metabolism in the malignant groups. It may also result from a lower protein content. Since the abundance of the human serum albumin protein is higher compared to other proteins in the blood serum, this decrease cannot be attributed to other proteins [73]. Therefore, this decrease can be connected with the decrease in serum albumin levels. Serum albumin provides a simple method for determining visceral protein function. Decreasing in inflammatory conditions, albumin is a well-known negative acute phase protein [74]. In cancer, both inflammation and malnutrition may suppress albumin synthesis, and hence, it is used to evaluate the patient nutritional status, cancer severity, progression, and prognosis [73,75,76]. Several studies have reported that there is no hypoalbuminemia in the early stages of cancer, but as the disease progresses albumin levels fall significantly [75–77].

The observed increase in the phosphate level of nucleic acids for malignant serum samples (LC, MPM) and the increase in nucleic acid/protein ratios of the diseased groups' serum samples (Fig. 2E) suggest an increased nucleic acid content in comparison to proteins in the patients. Supporting our study, an increase in the integrated area in the phosphates of nucleic acids for cervical cancer tissue samples was reported by FTIR microspectroscopy [78]. It was proposed that this deviation could be due to changes in the levels of either RNA or DNA, and they calculated RNA/DNA intensity ratios based on I(1121)/I(1020), as reported earlier by Argov et al. [79,80] for colon cancer. This ratio was found as higher in malignant samples than those in healthy tissues. In our study, since the serum samples do not show the band at 1020 cm^{-1} related to DNA, the other DNA band at 835 cm^{-1} was used to find out RNA/DNA area ratios (Table 3, Fig. 2F). RNA/DNA ratio for BE group remained almost the same as in control serum samples, while it tended to increase in malignant serum samples and it was found significantly higher in the serum samples of MPM patients, consistent with various cancer studies published by other groups [79,80]. The observed decrease in DNA concentration also showed that this increase in RNA/DNA ratio is due to the increase in RNA amount. The observed significant change in the RNA/DNA area ratio, especially in MPM, was an important spectral output of the present study. Circulating cell-free RNAs obtained from plasma and serum, in the form of either messenger RNA or microRNA, are promising biomarkers in the diagnosis of the malignancies including MPM [81,82]. We consider that our results related to RNA amount in the serum samples of MPM patients are in agreement with those findings. The gold standard for RNA quantification is real-time reverse transcription PCR, but in this type quantification, the isolation of circulating cell-free RNAs is needed. So, their clinical use as a cancer biomarker should be validated by multi-center research studies for standardized methodologies, particularly sampling and isolation techniques [81]. However, by IR spectroscopy, we can obtain the change in RNA amount directly without doing any preprocessing to the sample, and this change contributes to the identification of individuals who may have MPM disease, with the machine learning techniques used.

In cancer, there is a disturbed glucose metabolism favoring increased uptake and use of glucose by tumor cells, known as the Warburg effect. Those disturbances may include gluconeogenesis along with glycolysis and mitochondrial metabolism [83]. Louis et al. measured metabolic changes in plasma of lung cancer patients and demonstrated

significantly higher levels of glucose suggesting a possible activation of gluconeogenesis [84]. In our study, the result related to the carbohydrate level is in agreement with those of reported in the literature [83,84] (Fig. 2H). However, a review summarizing recent studies regarding novel metabolites for early lung tumor detection and evaluation of disease progression proposed significantly lower glucose levels in both lung tumor tissue and biofluid samples of lung cancer patients [85]. All these results reveal that further studies are required in this regard, including both disease and patient related factors such as histological subtype, disease stage, nutritional status, and comorbidities.

Based on all the compositional differences between the biomolecules of the MPM, LC, BE and control groups mentioned above, we can conclude that these differences contribute significantly to the differentiation of the groups from each other. We reported, for the first time, the spectral parameters such as the higher saturated lipid content, the presence of qualitatively longer hydrocarbon acyl chained lipids, the higher triglyceride-cholesterol ester amount and increased lipid/protein ratio in the serum of both LC and MPM groups relative to the healthy control and BE groups can be used as biomarkers in cancer diagnosis. The higher RNA/DNA ratio was found to be significant only for MPM group which can be used as a specific biomarker in the diagnosis of MPM. Such findings prove the diagnostic potential of serum IR spectroscopy in MPM diagnosis.

It is not easy to discriminate malignant pleural lesions from benign pleural lesions, and currently the reported sensitivity of MPM cytological diagnosis ranges from 30 % to 75 % [86]. Imaging techniques are non-specific in differentiating MPM and benign pleural pathologies. Although some blood tests such as soluble mesothelin-related proteins (SMPRs), megakaryocyte potentiating factor (MPF), circulating tumor cells (CTC), and circulating tumor DNA (ct-DNA) can be used as adjuncts, none have sufficient sensitivity to be utilized alone. The latter two provide high specificity, but poor sensitivity (e.g. 28 % sensitivity, 95 % specificity) for CTC and accuracy improves when cancer progresses to more advanced stages [87,88]. In the absence of reliable noninvasive diagnostic tests, currently, pleural biopsy remains the only standard diagnostic method for MPM. So, there is a critical need for a sensitive, specific, non-invasive, easily accessible and also cost-effective screening method to diagnose MPM patients at early stages in the high-risk areas, asbestos-exposed populations, and families with BAP1 germline mutations. Even if the key elements of an effective screening test are both sensitivity and specificity, sensitivity has a higher priority to ensure the lowest false-negative rate. In our test, when all groups were evaluated together using the SVM technique, lower sensitivity values were obtained for MPM prediction compared to other groups (Fig. 3), but this value is still higher than the aforementioned blood tests [87,88]. However, when MPM-BE or MPM-LC were evaluated separately, better sensitivity values were observed in comparison to the above-mentioned blood techniques (Fig. 6). Furthermore, the LDA technique, which is applied for the first time in this study for MPM diagnosis and its discrimination from lung cancer, benign exudates and healthy controls, presented noteworthy prediction/classification performance. For 4 different groups, LDA prediction was obtained with 87.5 % accuracy and for 3 different groups (BE, LC and MPM), the accuracy of the discrimination in the developed model was 82.93 %. The discrimination accuracy of LDA model was 94.12 % and 91.07 % for a two-group case (BE and MPM groups, LC and MPM groups, respectively). So, higher accuracy for the identification of MPM was acquired. LDA analysis performed in the spectral region (1300–800 cm^{-1}), where the nucleic acids associated bands are located, clearly showed that the changes in these bands contribute to identifying the group members with quite high accuracy.

Such findings also prove FTIR's promising potential for diagnosis with a higher accuracy. A rapid diagnostic serum test such as infrared spectroscopy would be beneficial by reducing current diagnosis times and increasing the chance of successful treatment. It was also previously reported that FTIR is a rapid, inexpensive, an easy-to-use, and operator-independent spectroscopic tool that can analyze even small amounts of samples with great potential as a screening and diagnostic tool for a range of diseases in the clinical setting [31,89,90].

Since FTIR spectroscopy detects very small molecular changes in the blood serum, it may give information about the changes related to tumor long before they become visible to the pathologists. Moreover, while the knowledge and experience of the pathologist in biopsy play an important role in diagnosis, in our method, the results are not dependent on the subjective observation of an operator, but rather on computational analyses of the spectra. Thus, all these inferences show the importance of our technique in early diagnosis.

Despite these promising results, our study has some limitations. Almost all of the lung cancers in the sample group are in the advanced stage (metastatic stage) and with the adenocarcinoma subtype. Moreover, data unavailability in terms of survival and smoking status (missing information of almost half of the patients) are another limitations of this study. So, we could not evaluate the correlation between markers identified and stages of malignancy or survival. However, our study can be a guide for future studies. Large-scale studies may be carried out using techniques combining FTIR and pattern recognition methods to investigate the parameters of a predictive model which comprehensively reflect the markers dependence on stages of malignancy or survival.

5. Conclusion

The results of the current study demonstrated the biomolecular composition and structural differences between the serum samples of the disease (BE, LC and MPM) and the control groups. These biomolecular changes have diagnostic significance and enable the discrimination of malignant samples from controls and benign ones. The alterations in lipid metabolism include the variation in length and saturation of the acyl chains, and the amount of carbonyl group in the fatty acid esters that were observed in the malignant serum samples. These variations contributed to the separation of the malign groups from benign ones. Furthermore, it has been shown that the lipid/protein ratio increased in the serum of both LC and MPM groups relative to the control and BE groups and that the serum of MPM patients has a higher RNA/DNA area ratio. These results are of clinical importance. The observed significant change in the RNA/DNA area ratio for the MPM group was an important spectral output of the present study. While all the lipid-related ratios can be used as biomarkers in malignant group diagnosis, the RNA/DNA ratio can be used as a biomarker for the diagnosis of MPM. A very successful separation of LC and MPM groups from the control group was obtained by PCA. Moreover, the MPM group was successfully differentiated from LC and BE serum samples. In this study, the generated classification models by SVM and, especially, by LDA identified the group members quite well not only for controls but also for LC and MPM compared to the methods using traditional blood tests. The value of our present study comes from the examination of blood serum samples that are readily available in each individual, regardless of pleural fluid status. Since pleural fluid occurs at the late stages of cancer, an early diagnosis from easily collected blood serum is a very valuable approach. All the results of the present study point out a potential value of serum-based FTIR spectroscopy technique for serving as a screening tool targeting those having a history of asbestos exposure. The structural studies as in the current study with easily accessible biofluids such as serum will have significant contributions to better understand the diseases, their progression, and the effect of chemotherapeutics.

CRediT authorship contribution statement

Dilek Yonar: Conceptualization, Methodology, Validation, Investigation, Writing – original draft, Visualization. **Mete Severcan:** Validation, Formal analysis, Writing – review & editing. **Rafig Gurbanov:**

Formal analysis, Writing – review & editing. **Abdulsamet Sandal:** Resources, Validation, Writing – review & editing. **Ulku Yilmaz:** Resources. **Salih Emri:** Conceptualization, Resources, Writing – review & editing, Project administration, Funding acquisition. **Feride Severcan:** Conceptualization, Methodology, Validation, Supervision, Writing – review & editing.

Declaration of competing interest

The authors declare the following financial interests/personal relationships which may be considered as potential competing interests: Salih Emri reports financial support was provided by The Scientific and Technological Research Council of Turkey (TUBITAK).

Data availability

Data will be made available on request.

Acknowledgement

We would like to thank TUBITAK, The Scientific and Technological Research Council of Turkey, for providing financial support to the project numbered SBAG-113S294.

Appendix A. Supplementary data

Supplementary data to this article can be found online at https://doi.org/10.1016/j.bbadis.2022.166473.

References

[1] M. Carbone, S. Emri, A.U. Dogan, I. Steele, M. Tuncer, H.I. Pass, Y.I. Baris, A mesothelioma epidemic in Cappadocia: scientific developments and unexpected social outcomes, Nat. Rev. Cancer 7 (2007) 147–154, https://doi.org/10.1038/nrc2068.

[2] J.C. Wagner, C.A. Sleggs, P. Marchand, Diffuse pleural mesothelioma and Asbestos exposure in the North Western Cape Province, Occup. Environ. Med. 17 (1960) 260–271, https://doi.org/10.1136/oem.17.4.260.

[3] M.T. Milano, H. Zhang, Malignant pleural mesothelioma: a population-based study of survival, J. Thorac. Oncol. 5 (2010) 1841–1848, https://doi.org/10.1097/JTO.0b013e3181f1cf2b.

[4] M. Carbone, S.T. Arron, B. Beutler, A. Bononi, W. Cavenee, J.E. Cleaver, C. M. Croce, A. D'Andrea, W.D. Foulkes, G. Gaudino, J.L. Groden, E.P. Henske, I. D. Hickson, P.M. Hwang, R.D. Kolodner, T.W. Mak, D. Malkin, R.J. Monnat, F. Novelli, H.I. Pass, J.H. Petrini, L.S. Schmidt, H. Yang, Tumour predisposition and cancer syndromes as models to study gene–environment interactions, Nat. Rev. Cancer (2020) 1–17, https://doi.org/10.1038/s41568-020-0265-y.

[5] V. Delgermaa, K. Takahashi, E.-K. Park, G.V. Le, T. Hara, T. Sorahan, Global mesothelioma deaths reported to the World Health Organization between 1994 and 2008, Bull. World Health Organ. 89 (2011) 716–724, https://doi.org/10.2471/BLT.11.086678.

[6] E. Hacikamiloğlu, M. Gültekin, G. Boztaş, S. Dündar, E.Simsek Utku, A. Kavak Ergün, A. Sevinc, S. Tütüncü, E. Seymen, Turkey cancer statistics. https://hsgm.saglik.gov.tr/depo/birimler/kanser-db/istatistik/2014-RAPOR._uzuuun.pdf, 2017.

[7] W. Zhang, X. Wu, L. Wu, W. Zhang, X. Zhao, Advances in the diagnosis, treatment and prognosis of malignant pleural mesothelioma, Ann. Transl. Med. 3 (2015) 182, https://doi.org/10.3978/j.issn.2305-5839.2015.07.03.

[8] B.P. Lanphear, C.R. Buncher, Latent period for malignant mesothelioma of occupational origin, J. Occup. Med. 34 (1992) 718–721.

[9] A. Scherpereel, I. Opitz, T. Berghmans, I. Psallidas, M. Glatzer, D. Rigau, P. Astoul, S. Bölükbas, J. Boyd, J. Coolen, C. De Bondt, D. De Ruysscher, V. Durieux, C. Faivre-Finn, D. Fennell, F. Galateau-Salle, L. Greillier, M.A. Hoda, W. Klepetko, A. Lacourt, P. McElnay, N.A. Maskell, L. Mutti, J.C. Pairon, P. Van Schil, J.P. van Meerbeeck, D. Waller, W. Weder, G. Cardillo, P.M. Putora, ERS/ESTS/EACTS/ESTRO guidelines for the management of malignant pleural mesothelioma, Eur. Respir. J. 55 (2020), https://doi.org/10.1183/13993003.00953-2019.

[10] J.E. Heffner, J.S. Klein, Recent advances in the diagnosis and management of malignant pleural effusions, Mayo Clin. Proc. 83 (2008) 235–250, https://doi.org/10.4065/83.2.235.

[11] C. Boutin, F. Rey, J. Gouvernet, J.R. Viallat, P. Astoul, V. Ledoray, Thoracoscopy in pleural malignant mesothelioma: a prospective study of 188 consecutive patients. Part 2: prognosis and staging, Cancer 72 (1993) 394–404, https://doi.org/10.1002/1097-0142(19930715)72:2<394::AID-CNCR2820720214>3.0.CO;2-5.

[12] M.J. Baker, J. Trevisan, P. Bassan, R. Bhargava, H.J. Butler, K.M. Dorling, P. R. Fielden, S.W. Fogarty, N.J. Fullwood, K.A. Heys, C. Hughes, P. Lasch, P. L. Martin-Hirsch, B. Obinaju, G.D. Sockalingum, J. Sulé-Suso, R.J. Strong, M. J. Walsh, B.R. Wood, P. Gardner, F.L. Martin, Using fourier transform IR spectroscopy to analyze biological materials, Nat. Protoc. 9 (2014) 1771–1791, https://doi.org/10.1038/nprot.2014.110.

[13] C. Krafft, G. Steiner, C. Beleites, R. Salzer, Disease recognition by infrared and raman spectroscopy, J. Biophotonics 2 (2009) 13–28, https://doi.org/10.1002/jbio.200810024.

[14] F. Severcan, P.I. Haris, Introduction to vibrational spectroscopy in diagnosis and screening, in: F. Severcan, P.I. Haris (Eds.), Vib. Spectrosc. Diagnosis Screen., Netherlands, 2012, pp. 1–11.

[15] K.B. Beć, J. Grabska, C.W. Huck, Near-infrared spectroscopy in bio-applications, Molecules 25 (2020), https://doi.org/10.3390/molecules25122948.

[16] J.N. Fernandes, L.M.B. Dos Santos, T. Chouin-Carneiro, M.G. Pavan, G.A. Garcia, M.R. David, J.C. Beier, F.E. Dowell, R. Maciel-de-Freitas, M.T. Sikulu-Lord, Rapid, noninvasive detection of zika virus in Aedes aegypti mosquitoes by near-infrared spectroscopy, Sci. Adv. 4 (2018), https://doi.org/10.1126/sciadv.aat0496.

[17] S. Mordechai, E. Shufan, B.S. Porat Katz, A. Salman, Early diagnosis of Alzheimer's disease using infrared spectroscopy of isolated blood samples followed by multivariate analyses, Analyst 142 (2017) 1276–1284, https://doi.org/10.1039/C6AN01580H.

[18] D. Yonar, L. Ocek, B.I. Tiftikcioglu, Y. Zorlu, F. Severcan, Relapsing-remitting multiple sclerosis diagnosis from cerebrospinal fluids via fourier transform infrared spectroscopy coupled with multivariate analysis, Sci. Rep. 8 (2018) 1025, https://doi.org/10.1038/s41598-018-19303-3.

[19] V. Rai, R. Mukherjee, A. Routray, A.K. Ghosh, S. Roy, B.P. Ghosh, P.B. Mandal, S. Bose, C. Chakraborty, Serum-based diagnostic prediction of oral submucous fibrosis using FTIR spectrometry, Spectrochim. Acta A Mol. Biomol. Spectrosc. 189 (2018) 322–329, https://doi.org/10.1016/j.saa.2017.08.018.

[20] D. Naumann, H. Fabian, P. Lasch, FTIR spectroscopy of cells, tissues and body fluids, in: A. Barth, P.I. Haris (Eds.), Biol. Biomed. Infrared Spectrosc, IOS Press, 2009, pp. 312–354, https://doi.org/10.3233/978-1-60750-045-2-312.

[21] E.F. Petricoin, C. Belluco, R.P. Araujo, L.A. Liotta, The blood peptidome: a higher dimension of information content for cancer biomarker discovery, Nat. Rev. Cancer 6 (2006), https://doi.org/10.1038/nrc2011.

[22] J.R. Hands, K.M. Dorling, P. Abel, K.M. Ashton, A. Brodbelt, C. Davis, T. Dawson, M.D. Jenkinson, R.W. Lea, C. Walker, M.J. Baker, Attenuated Total reflection fourier transform infrared (ATR-FTIR) spectral discrimination of brain tumour severity from serum samples, J. Biophotonics 7 (2014) 189–199, https://doi.org/10.1002/jbio.201300149.

[23] X. Sun, Y. Xu, J. Wu, Y. Zhang, K. Sun, Detection of lung cancer tissue by attenuated total reflection-fourier transform infrared spectroscopy - a pilot study of 60 samples, J. Surg. Res. 179 (2013), https://doi.org/10.1016/j.jss.2012.08.057.

[24] K. Gajjar, J. Trevisan, G. Owens, P.J. Keating, N.J. Wood, H.F. Stringfellow, P. L. Martin-Hirsch, F.L. Martin, Fourier-transform infrared spectroscopy coupled with a classification machine for the analysis of blood plasma or serum: a novel diagnostic approach for ovarian cancer, Analyst 138 (2013) 3917, https://doi.org/10.1039/c3an36654e.

[25] X. Wang, X. Shen, D. Sheng, X. Chen, X. Liu, FTIR spectroscopic comparison of serum from lung cancer patients and healthy persons, Spectrochim. Acta A Mol. Biomol. Spectrosc. 122 (2014) 193–197, https://doi.org/10.1016/j.saa.2013.11.049.

[26] P.D. Lewis, K.E. Lewis, R. Ghosal, S. Bayliss, A.J. Lloyd, J. Wills, R. Godfrey, P. Kloer, L.A. Mur, Evaluation of FTIR spectroscopy as a diagnostic tool for lung cancer using sputum, BMC Cancer 10 (2010) 640, https://doi.org/10.1186/1471-2407-10-640.

[27] B.R. Wood, L. Chiriboga, H. Yee, M.A. Quinn, D. McNaughton, M. Diem, Fourier transform infrared (FTIR) spectral mapping of the cervical transformation zone, and dysplastic squamous epithelium, Gynecol. Oncol. 93 (2004) 59–68, https://doi.org/10.1016/j.ygyno.2003.12.028.

[28] J. Backhaus, R. Mueller, N. Formanski, N. Szlama, H.-G. Meerpohl, M. Eidt, P. Bugert, Diagnosis of breast cancer with infrared spectroscopy from serum samples, Vib. Spectrosc. 52 (2010) 173–177, https://doi.org/10.1016/J.VIBSPEC.2010.01.013.

[29] G. Theophilou, K.M.G. Lima, P.L. Martin-Hirsch, H.F. Stringfellow, F.L. Martin, ATR-FTIR spectroscopy coupled with chemometric analysis discriminates normal, borderline and malignant ovarian tissue: classifying subtypes of human cancer, Analyst 141 (2016) 585–594, https://doi.org/10.1039/C5AN00939A.

[30] J. Ollesch, M. Heinze, H.M. Heise, T. Behrens, T. Brüning, K. Gerwert, It's in your blood: spectral biomarker candidates for urinary bladder cancer from automated FTIR spectroscopy, J. Biophotonics 7 (2014) 210–221, https://doi.org/10.1002/jbio.201300163.

[31] S. Gok, O.Z. Aydin, Y.S. Sural, F. Zorlu, U. Bayol, F. Severcan, Bladder cancer diagnosis from bladder wash by fourier transform infrared spectroscopy as a novel test for tumor recurrence, J. Biophotonics 9 (2016) 967–975, https://doi.org/10.1002/jbio.201500322.

[32] E. Gazi, J. Dwyer, P. Gardner, A. Ghanbari-Siahkali, A. Wade, J. Miyan, N. Lockyer, J. Vickerman, N. Clarke, J. Shanks, L. Scott, C. Hart, M. Brown, Applications of fourier transform infrared microspectroscopy in studies of benign prostate and prostate cancer. A pilot study, J. Pathol. 201 (2003) 99–108, https://doi.org/10.1002/path.1421.

[33] C. Lima, V. Goulart, L. Côrrea, T. Pereira, D. Zezell, ATR-FTIR spectroscopy for the assessment of biochemical changes in skin due to cutaneous squamous cell carcinoma, Int. J. Mol. Sci. 16 (2015) 6621–6630, https://doi.org/10.3390/ijms16046621.

[34] E. Kaznowska, J. Depciuch, K. Szmuc, J. Cebulski, Use of FTIR spectroscopy and PCA-LDC analysis to identify cancerous lesions within the human colon, J. Pharm. Biomed. Anal. 134 (2017) 259–268, https://doi.org/10.1016/j.jpba.2016.11.047.

[35] H.P. Wang, H.-C. Wang, Y.-J. Huang, Microscopic FTIR studies of lung cancer cells in pleural fluid, Sci. Total Environ. 204 (1997) 283–287, https://doi.org/10.1016/S0048-9697(97)00180-0.

[36] K. Yano, S. Ohoshima, Y. Gotou, K. Kumaido, T. Moriguchi, H. Katayama, Direct measurement of human lung cancerous and noncancerous tissues by fourier transform infrared microscopy: can an infrared microscope be used as a clinical Tool? Anal. Biochem. 287 (2000) 218–225, https://doi.org/10.1006/ABIO.2000.4872.

[37] R. Bangaoil, A. Santillan, L.M. Angeles, L. Abanilla, A. Lim, M. Cristina Ramos, A. Fellizar, L. Guevarra, P.M. Albano, ATR-FTIR spectroscopy as adjunct method to the microscopic examination of hematoxylin and eosin-stained tissues in diagnosing lung cancer, PLoS One 15 (2020), https://doi.org/10.1371/journal.pone.0233626.

[38] F. Großerueschkamp, T. Bracht, H.C. Diehl, C. Kuepper, M. Ahrens, A. Kallenbach-Thieltges, A. Mosig, M. Eisenacher, K. Marcus, T. Behrens, T. Brüning, D. Theegarten, B. Sitek, K. Gerwert, Spatial and molecular resolution of diffuse malignant mesothelioma heterogeneity by integrating label-free FTIR imaging, laser capture microdissection and proteomics, Sci. Rep. 7 (2017) 44829, https://doi.org/10.1038/srep44829.

[39] S. Abbas, N.S. Ozek, S. Emri, D. Koksal, M. Severcan, F. Severcan, Diagnosis of malignant pleural mesothelioma from pleural fluid by fourier transform-infrared spectroscopy coupled with chemometrics (Erratum), J. Biomed. Opt. 23 (2018) 1, https://doi.org/10.1117/1.JBO.23.10.109801.

[40] E.P. Cantey, J.M. Walter, T. Corbridge, J.H. Barsuk, Complications of thoracentesis: incidence, risk factors, and strategies for prevention, Curr. Opin. Pulm. Med. 22 (2016), https://doi.org/10.1097/MCP.0000000000000285.

[41] M. Medenica, M. Medenica, D. Cosovic, Pleural effusions in lung cancer: detection and treatment, Lung Cancer - Strateg. Diagn. Treat. (2018), https://doi.org/10.5772/intechopen.78307.

[42] A. Noor Husain T. V Colby N.G. Or ō nez T. Craig Allen R. Luther Attanoos M. Beth Beasley K. Jo Butnor L.R. Chirieac A.M. Churg S. Dacic F. Coise Galateau-Salí A. Gibbs A.M. Gown T. Krausz L. Anne Litzky A. Marchevsky A.G. Nicholson V. Louis Roggli A.K. Sharma W.D. Travis A.E. Walts M.R. Wick, EARLY ONLINE RELEASE Guidelines for Pathologic Diagnosis of Malignant Mesothelioma 2017 Update of the Consensus Statement From the International Mesothelioma Interest Group, (n. d.). doi:10.5858/arpa.2017-0124-RA.

[43] R.W. Light, M.I. Macgregor, P.C. Luchsinger, W.C. Ball, Pleural effusions: the diagnostic separation of transudates and exudates, Ann. Intern. Med. 77 (1972) 507–513. http://www.ncbi.nlm.nih.gov/pubmed/4642731. (Accessed 2 February 2019).

[44] M. Vives, J.M. Porcel, M. Vicente de Vera, E. Ribelles, M. Rubio, A study of Light's criteria and possible modifications for distinguishing exudative from transudative pleural effusions, Chest 109 (1996) 1503–1507. http://www.ncbi.nlm.nih.gov/pubmed/8769501. (Accessed 13 November 2017).

[45] G. Cakmak, F. Zorlu, M. Severcan, F. Severcan, Screening of protective effect of amifostine on radiation-induced structural and functional variations in rat liver microsomal membranes by FT-IR spectroscopy, Anal. Chem. 83 (2011) 2438–2444, https://doi.org/10.1021/ac102043p.

[46] L. Wang, B. Mizaikoff, Application of multivariate data-analysis techniques to biomedical diagnostics based on mid-infrared spectroscopy, Anal. Bioanal. Chem. 391 (2008), https://doi.org/10.1007/s00216-008-1989-9.

[47] K.H. Esbensen, Multivariate Data Analysis: In Practice: an Introduction to Multivariate Data Analysis and Experimental Design, 5th ed., CAMO Software, Esbjerg, 2010.

[48] D. Ballabio, R. Todeschini, Multivariate classification for qualitative analysis, in: D.-W. Sun (Ed.), Infrared Spectrosc. Food Qual. Anal. Control, Elsevier, Ireland, 2009, pp. 83–104.

[49] T. Hastie, R. Tibshirani, J. Friedman, Springer Series in Statistics The Elements of Statistical Learning - Data Mining, Inference, and Prediction, 2009.

[50] A. Steinwart, Ingo Christmann, Support Vector Machines, 1st ed., Springer-Verlag New York, New York, 2008.

[51] B. Palumbo, M.L. Fravolini, T. Buresta, F. Pompili, N. Forini, P. Nigro, P. Calabresi, N. Tambasco, Diagnostic accuracy of parkinson disease by support vector machine (SVM) analysis of 123I-FP-CIT brain SPECT data, Med. (United States) 93 (2014), https://doi.org/10.1097/MD.0000000000000228.

[52] R. Gurbanov, S. Tunçer, S. Mingu, F. Severcan, A.G. Gozen, Methylation, sugar puckering and Z-form status of DNA from a heavy metal-acclimated freshwater gordonia sp, J. Photochem. Photobiol. B Biol. (2019) 198, https://doi.org/10.1016/j.jphotobiol.2019.111580.

[53] A. Dogan, R. Gurbanov, M. Severcan, F. Severcan, CoronaVac (Sinovac) COVID-19 vaccine-induced molecular changes in healthy human serum by infrared spectroscopy coupled with chemometrics, Turk. J. Biol. 45 (2021), https://doi.org/10.3906/biy-2105-65.

[54] M. Khanmohammadi, R. Nasiri, K. Ghasemi, S. Samani, A. Bagheri Garmarudi, Diagnosis of basal cell carcinoma by infrared spectroscopy of whole blood samples applying soft independent modeling class analogy, J. Cancer Res. Clin. Oncol. 133 (2007) 1001–1010, https://doi.org/10.1007/s00432-007-0286-x.

[55] G. Bellisola, C. Sorio, Infrared spectroscopy and microscopy in cancer research and diagnosis, Am. J. Cancer Res. 2 (2012) 1–21.

[56] B.R. Wood, The importance of hydration and DNA conformation in interpreting infrared spectra of cells and tissues, Chem. Soc. Rev. 45 (2016), https://doi.org/10.1039/c5cs00511f.

[57] F. Kucuk Baloglu, S. Garip, S. Heise, G. Brockmann, F. Severcan, FTIR imaging of structural changes in visceral and subcutaneous adiposity and brown to white adipocyte transdifferentiation, Analyst 140 (2015) 2205–2214, https://doi.org/10.1039/c4an02008a.

[58] D. Sheng, Y. Wu, X. Wang, D. Huang, X. Chen, X. Liu, Comparison of serum from gastric cancer patients and from healthy persons using FTIR spectroscopy, Spectrochim. Acta - Part A Mol. Biomol. Spectrosc. 116 (2013) 365–369, https://doi.org/10.1016/j.saa.2013.07.055.

[59] P. Mega Tiber, O. Orun, C. Nacar, U.O. Sezerman, F. Severcan, M. Severcan, A. Matagne, B. Kan, Structural characterization of recombinant bovine Goα by spectroscopy and homology modeling, Spectroscopy 26 (2011), https://doi.org/10.3233/SPE-2011-0543.

[60] N. Fujioka, Y. Morimoto, T. Arai, M. Kikuchi, Discrimination between normal and malignant human gastric tissues by fourier transform infrared spectroscopy, Cancer Detect. Prev. 28 (2004) 32–36, https://doi.org/10.1016/j.cdp.2003.11.004.

[61] J. Titus, E. Viennois, D. Merlin, A.G. Unil Perera, Minimally invasive screening for colitis using attenuated total internal reflectance fourier transform infrared spectroscopy, J. Biophotonics 10 (2017) 465–472, https://doi.org/10.1002/jbio.201600041.

[62] H. Ghimire, M. Venkataramani, Z. Bian, Y. Liu, A.G.U. Perera, ATR-FTIR spectral discrimination between normal and tumorous mouse models of lymphoma and melanoma from serum samples, Sci. Rep. 7 (2017), https://doi.org/10.1038/s41598-017-17027-4.

[63] C. Petibois, V. Rigalleau, A.-M. Melin, A. Perromat, G. Cazorla, H. Gin, G. Déléris, Determination of glucose in dried serum samples by fourier-transform infrared spectroscopy, Clin. Chem. 45 (1999).

[64] E. Schillebeeckx, J.P. van Meerbeeck, K. Lamote, Clinical utility of diagnostic biomarkers in malignant pleural mesothelioma: a systematic review and meta-analysis, Eur. Respir. Rev. 30 (2021), https://doi.org/10.1183/16000617.0057-2021.

[65] B. Wiederhold, O. Amr, P. Modi, Thoracentesis, StatPearls Publishing, Treasure Island (FL), 2022. https://www.ncbi.nlm.nih.gov/books/NBK441866/.

[66] J. Falleti, M. Giordano, I. Cozzolino, A. Vetrani, A. De Renzo, P. Zeppa, Cutaneous needle track seeding of mesothelioma diagnosed by fine needle aspiration cytology: a case report, Acta Cytol. 54 (2010).

[67] F. Baenke, B. Peck, H. Miess, A. Schulze, Hooked on fat: the role of lipid synthesis in cancer metabolism and tumour development, DMM Dis. Model. Mech. 6 (2013) 1353–1363, https://doi.org/10.1242/dmm.011338.

[68] J. Long, C.-J. Zhang, N. Zhu, K. Du, Y.-F. Yin, X. Tan, D.-F. Liao, L. Qin, Lipid metabolism and carcinogenesis, cancer development, Am. J. Cancer Res. 8 (2018) 778–791. http://www.ncbi.nlm.nih.gov/pubmed/29888102. (Accessed 22 December 2019).

[69] E.W. Gabrielson, M.L. Pinn, J.R. Testa, F.P. Kuhajda, Increased fatty acid synthase is a therapeutic target in mesothelioma, Clin. Cancer Res. 7 (2001) 153–157. http://www.ncbi.nlm.nih.gov/pubmed/11205903. (Accessed 25 December 2019).

[70] S. Ravipati, D.R. Baldwin, H.L. Barr, A.W. Fogarty, D.A. Barrett, Plasma lipid biomarker signatures in squamous carcinoma and adenocarcinoma lung cancer patients, Metabolomics 11 (2015) 1600–1611, https://doi.org/10.1007/s11306-015-0811-x.

[71] L.J. Wei, C. Zhang, H. Zhang, X. Wei, S.X. Li, J.T. Liu, X.B. Ren, A case-control study on the association between serum lipid level and the risk of breast cancer, Zhonghua Yu Fang Yi Xue Za Zhi 50 (2016) 1091–1095, https://doi.org/10.3760/cma.j.issn.0253-9624.2016.12.013.

[72] D.J. Murphy, R.R. Gill, Overview of treatment related complications in malignant pleural mesothelioma, Ann. Transl. Med. 5 (2017), https://doi.org/10.21037/atm.2017.03.97.

[73] Y. Jin, L. Zhao, F. Peng, Prognostic impact of serum albumin levels on the recurrence of stage I non-small cell lung cancer, Clinics 68 (2013) 686–693, https://doi.org/10.6061/clinics/2013(05)17.

[74] C. Gabay, I. Kushner, Acute-phase proteins and other systemic responses to inflammation, N. Engl. J. Med. 340 (1999) 448–454, https://doi.org/10.1056/NEJM199902113400607.

[75] D. Gupta, C.G. Lis, Pretreatment serum albumin as a predictor of cancer survival: a systematic review of the epidemiological literature, Nutr. J. 9 (2010), https://doi.org/10.1186/1475-2891-9-69.

[76] S.W.D. Merriel, R. Carroll, F. Hamilton, W. Hamilton, Association between unexplained hypoalbuminaemia and new cancer diagnoses in UK primary care patients, Fam. Pract. 33 (2016) 449–452, https://doi.org/10.1093/fampra/cmw051.

[77] H.-K. Kao, W.F. Chen, C.-H. Chen, V.B.-H. Shyu, M.-H. Cheng, K.-P. Chang, The roles of albumin levels in head and neck cancer patients with liver cirrhosis undergoing tumor ablation and microsurgical free tissue transfer, PLoS One 7 (2012), e52678, https://doi.org/10.1371/journal.pone.0052678.

[78] S. Mordechai, R.K. Sahu, Z. Hammody, S. Mark, K. Kantarovich, H. Guterman, A. Podshyvalov, J. Goldstein, S. Argov, Possible common biomarkers from FTIR microspectroscopy of cervical cancer and melanoma, J. Microsc. 215 (2004) 86–91, https://doi.org/10.1111/j.0022-2720.2004.01356.x.

[79] S. Argov, J. Ramesh, A. Salman, I. Sinelnikov, J. Goldstein, H. Guterman, S. Mordechai, Diagnostic potential of fourier-transform infrared microspectroscopy and advanced computational methods in colon cancer patients, J. Biomed. Opt. 7 (2002) 248, https://doi.org/10.1117/1.1463051.

[80] R.K. Sahu, A. Salman, S. Mordechai, Tracing overlapping biological signals in mid-infrared using colonic tissues as a model system, World J. Gastroenterol. 23 (2017), https://doi.org/10.3748/wjg.v23.i2.286.

[81] K.W.E. Cheung, S.Yu R. Choi, L.T.C. Lee, N.L.E. Lee, H.F. Tsang, Y.T. Cheng, W.C. S. Cho, E.Y.L. Wong, S.C.C. Wong, The potential of circulating cell free RNA as a biomarker in cancer, Expert Rev. Mol. Diagn. 19 (2019), https://doi.org/10.1080/14737159.2019.1633307.

[82] I. Cavallari, L. Urso, E. Sharova, G. Pasello, V. Ciminale, Liquid biopsy in malignant pleural mesothelioma: state of the art, pitfalls, and perspectives, Front. Oncol. 9 (2019), https://doi.org/10.3389/fonc.2019.00740.
[83] K. Vanhove, G.-J. Graulus, L. Mesotten, M. Thomeer, E. Derveaux, J.-P. Noben, W. Guedens, P. Adriaensens, The metabolic landscape of lung cancer: new insights in a disturbed glucose metabolism, Front. Oncol. 9 (2019) 1215, https://doi.org/10.3389/fonc.2019.01215.
[84] E. Louis, P. Adriaensens, W. Guedens, T. Bigirumurame, K. Baeten, K. Vanhove, K. Vandeurzen, K. Darquennes, J. Vansteenkiste, C. Dooms, Z. Shkedy, L. Mesotten, M. Thomeer, Detection of lung cancer through metabolic changes measured in blood plasma, J. Thorac. Oncol. 11 (2016) 516–523, https://doi.org/10.1016/j.jtho.2016.01.011.
[85] S. Bamji-Stocke, V. van Berkel, D.M. Miller, H.B. Frieboes, A review of metabolism-associated biomarkers in lung cancer diagnosis and treatment, Metabolomics 14 (2018), https://doi.org/10.1007/s11306-018-1376-2.
[86] R. Bruno, G. Alì, A.M. Poma, A. Proietti, R. Libener, N. Mariani, C. Niccoli, A. Chella, A. Ribechini, F. Grosso, G. Fontanini, Differential diagnosis of malignant pleural mesothelioma on cytology, J. Mol. Diagn. 22 (2020), https://doi.org/10.1016/j.jmoldx.2019.12.009.
[87] H.I. Pass, M. Alimi, M. Carbone, H. Yang, C.M. Goparaju, Mesothelioma biomarkers: a review highlighting contributions from the early detection research network, Cancer Epidemiol. Biomark. Prev. 29 (2020), https://doi.org/10.1158/1055-9965.EPI-20-0083.
[88] K. Yoneda, F. Tanaka, N. Kondo, M. Hashimoto, T. Takuwa, S. Matsumoto, Y. Okumura, N. Tsubota, A. Sato, T. Tsujimura, C. Tabata, T. Nakano, S. Hasegawa, Blood tests in malignant pleural mesothelioma (MPM), J. Clin. Oncol. 32 (2014), https://doi.org/10.1200/jco.2014.32.15_suppl.7582.
[89] H.J. Butler, P.M. Brennan, J.M. Cameron, D. Finlayson, M.G. Hegarty, M. D. Jenkinson, D.S. Palmer, B.R. Smith, M.J. Baker, Development of high-throughput ATR-FTIR technology for rapid triage of brain cancer, Nat. Commun. 10 (2019), https://doi.org/10.1038/s41467-019-12527-5.
[90] J.M. Cameron, C. Rinaldi, H.J. Butler, M.G. Hegarty, P.M. Brennan, M. D. Jenkinson, K. Syed, K.M. Ashton, T.P. Dawson, D.S. Palmer, M.J. Baker, Stratifying brain tumour histological sub-types: the application of ATR-FTIR serum spectroscopy in secondary care, Cancers (Basel) 12 (2020), https://doi.org/10.3390/cancers12071710.